Atmospheric chemistry regimes in intercontinental air traffic corridors: Ozone versus NO_x sensitivity

Richard G. Derwent[1,*], Monica Dosa[2], M. Anwar H. Khan[2], Rayne Holland[2] and Dudley E. Shallcross[2]

[1]rdscientific, Newbury, UK

[2]Atmospheric Chemistry Research Group, School of Chemistry, University of Bristol, Bristol, UK

*Corresponding Author.

e-mail address: r.derwent@btopenworld.com (R.G.Derwent)

Abstract

This study focusses on the environmental consequences of aircraft NO_x emissions and their role and impact on ozone formation in the upper troposphere and lower stratosphere (UTLS). We use a global chemistry transport/box model approach to quantify the impacts of NO_x on UTLS ozone over time scales of hours and over distance scales appropriate to air traffic corridors and aircraft flight paths. An important feature of our study has been to provide a marked contrast to the coarse spatial resolution of the global model studies typically employed to assess the impacts of aviation NO_x on UTLS ozone. Real operational aviation routing data are used to quantify the NO_x impacts on ozone at 235 locations on 21 flight paths. The NO_x impact on ozone in the intercontinental air traffic corridors is strongest in the great circle routes from North America and Europe into Asia and weakest in the trans-polar routes. The NO_x impacts identified with the CTM/box model combination are significantly smaller compared with those identified in the current global models typically used to assess aviation NO_x impacts. Further research is required to confirm our assessment of those flight paths that appear to show greatest NO_x – O_3 impacts and those the least and extend our analyses into the tropics and southern hemisphere.

1. Introduction

There is much current interest from policy-makers in the global-scale environmental impacts of aviation and how the aviation industry will cope with the shift to low- or zero-carbon futures (for example: IATA, 2023; Transport & Environment, 2018). These global scale impacts include global climate change driven by emissions of carbon dioxide and oxides of nitrogen (NO_x), cirrus cloud formation, soot emissions and contrail formation (IPCC, 2018; Lee et al., 2021,2023; and the references therein). In this study, our interest lies in the environmental consequences of aircraft NO_x emissions and their role and impact on ozone (O_3) formation in the upper troposphere and lower stratosphere (UTLS). The impact of aviation NO_x emissions on tropospheric O_3 has two components with distinctly different time-scales (Wild and Prather, 2000). The first component is a rapid O_3 production which occurs over a time-scale of hours to days. The second component leads to net O_3 destruction, builds up over months, decays away over several years and is driven by the impact of NO_x on the hydroxyl radical (OH) – methane – O_3 chemistry. Aviation NO_x is not alone in showing this two-component behaviour which is also shown by ground-level NO_x emissions (Wild et al. 2001), hydrogen (Derwent et al., 2020) and organic compounds

(Derwent et al., 2023). This study addresses only the first, rapid and direct impact of NO_x on O_3. It is understood that this is only one aspect of the larger global aviation impact story.

An unintended consequence of any present or future aircraft propulsion system based on combustion is the emission of NO_x, irrespective of the fuel combusted whether fossil fuel-based, biofuel-derived (Transport & Environment, 2018; Lee et al., 2023) or hydrogen (Transport & Environment, 2023). It is conceivable that O_3 formation from NO_x can be mitigated by rerouting aircraft corridors, formation flying and other options (Khan et al., 2023). Whether any of these mitigation options would actually reduce the climate consequences of ozone formation in the real atmosphere will depend on the adequacy and completeness of the current global chemistry-transport models (CTMs) and the representation of the atmospheric O_3-NO_x chemistry upon which they depend. Because of the uncertainties in assessment models, it has been difficult to recommend definitive policy actions because of their limited impacts and perhaps unintended consequences (Lee et al., 2021). If it is acknowledged that there are considerable uncertainties in assessment models, then an important issue is the extent to which further research could narrow these uncertainties. Carslaw et al., (2018) have recognised this issue in the context of climate models and climate science. Understanding uncertainty in the models of NO_x impacts on UTLS ozone is the main motivation behind this study.

Here, a CTM/box model approach is employed to quantify the impacts of aviation NO_x on UTLS ozone over timescales of hours and distance scales appropriate to flightpaths. An important feature of our study is the marked contrast between these time and spatial scales offered by the CTM/box model approach and those offered by the current CTMs typically used to assess impacts of global aviation. The global CTM models typically used in studies of aircraft NO_x emissions are coarse scale models when viewed from the aspect of an individual aircraft flight path. The emission grids are typically several hundreds of kilometres in scale and aircraft NO_x emissions are instantly mixed throughout these emission grid squares over timescales of months. However, in the real atmosphere it would take many hours for the aircraft NO_x emissions to mix across distances of the order of hundreds of km during which time NO_x levels would have decayed away through the action of the photochemistry. The result is that the NO_x – O_3 impacts estimated using global CTMs may not describe accurately the real situation in the intercontinental air traffic corridors and may lead to the overestimation of the impact of aircraft NO_x emissions on UTLS ozone as shown by comparison with the CTM/box model approach adopted here. Further research is recommended to confirm our assessment of those air traffic corridors that appear to show greatest NO_x – O_3 impacts and those the least.

2. Methods

2.1 Flight-path information

Details of the flight paths taken by commercial aviation were taken from the open-source air traffic data set Open Sky (https://opensky-network.org). The OpenSky Network sources data from Automatic Dependent Surveillance-Broadcast (ADS-B) ground-based crowdsourced receivers which determine aircraft latitude, longitude and altitude, along with additional measurements such as flight track and ground speed, at a temporal resolution of one second.

We focussed on twenty-one intercontinental flight paths, eleven of which left Europe bound for North America and Asia and ten left Asia for North America and Europe, as detailed in Table 1. All these flight paths stayed within the northern hemisphere and within the latitude range from 22^{o} to 84^{o} N. The locations of the flight paths were noted at hourly intervals in the Open Sky data sets. These flight paths present a reasonable coverage of northern hemisphere mid-latitudes as shown in the location map In Figure 1.

2.2 Atmospheric chemistry of ozone versus NO_x sensitivity in the UTLS

It is well understood that atmospheric photochemical O_3 formation rate, PO_3, is dependent on the availability of NO_x (Chameides and Walker, 1973; Crutzen, 1973). In the polluted atmospheric boundary layer, photochemical O_3 formation can be described as NO_x- or VOC-sensitive if reductions in NO_x or volatile organic compounds (VOCs) give greater or lesser reductions in O_3 (Sillman et al., 1990). In low-NO_x conditions, increasing NO_x promotes photochemical O_3 formation by promoting the reaction of the hydroperoxy (HO_2) radical with nitric oxide (NO) in reaction (1) over its self-reaction leading to radical loss in reaction (2):

$HO_2 + NO \rightarrow OH + NO_2$ (1)

$HO_2 + HO_2 \rightarrow H_2O_2 + O_2$ (2)

and O_3 formation is said to be NO_x-sensitive or NO_x-limited, whilst changes in VOCs have little impact. Ultimately as NO_x levels increase, photochemical ozone formation is inhibited by hydroxyl (OH) radical loss through its reaction with nitrogen dioxide (NO_2) in reaction (3):

$OH + NO_2 + M \rightarrow HNO_3 + M$ (3)

and photochemical ozone formation becomes increasingly sensitive to VOCs, relatively insensitive to NO_x levels and ultimately decreases with increasing NO_x. O_3 formation is then said to be VOC-limited or VOC-sensitive or NO_x-saturated (Sillman, 1999).

The use of the photochemical O_3 production rate, PO_3, and its response to reductions in NO_x versus VOCs, as an indicator of atmospheric chemistry regime is not without drawbacks. One such drawback is its essential reliance on air quality modelling, ruling it out as an observations-based approach. As a consequence, a number of indicator species ratios have been developed with a view to the diagnosis of atmospheric chemistry regime in the polluted atmospheric boundary layer in the base case (or from observations) without the need for the additional NO_x and VOC reduction scenario cases. These indicator species ratios include O_3/NO_z, where NO_z = HNO_3 + PAN + nitrate aerosol, $HCHO/NO_2$, H_2O_2/HNO_3 and α^{CH3O2} (Sillman, 1995; Jaegle, et al., 1998; Nussbaumer et al., 2023). Sillman (1995) proposed the indicator ratio HCHO/NOy which compares the reaction of OH with VOCs, leading to HCHO and enhancing O_3 formation, in competition with radical loss through OH + NO_2 in reaction (3). The indicator ratio H_2O_2/NO_y was also proposed by Sillman (1995) which compares the loss of HO_2 radicals in reaction (2) with the loss of OH radicals in reaction (3). The α^{CH3O2} metric provides a relatively recent method of defining NO_x- and VOC-sensitivity based on the fate of methyl peroxy (CH_3O_2) radicals forming HCHO by reaction with NO in reaction (4) and (5) versus radical loss through reaction with HO_2 in reaction (5), (Nussbaumer et al., 2023):

$CH_3O_2 + NO \rightarrow CH_3O + NO_2$ (4)

$CH_3O + O_2 \rightarrow HCHO + HO_2$ (5).

In the paragraphs that follow, these indicator species ratios are evaluated against PO_3 for their specificity and applicability to locations within the intercontinental air traffic corridors.

In this study, a combination of a global chemistry-transport model (CTM) and a box model are employed in the study of the impact of aviation NO_x emissions on O_3 levels in the upper troposphere – lower stratosphere (UTLS) region, the atmospheric region where O_3 changes exert a dramatic impact on radiative forcing and climate change. We build confidence in our CTM/box model approach by investigating how the concepts of NO_x-sensitive and VOC-sensitive can be applied successfully in the UTLS region through detailed comparisons with the indicator species ratios: O_3/NO_z, $HCHO/NO_2$, H_2O_2/HNO_3 and α^{CH3O2}.

2.3 STOCHEM-CRI model

A state-of-the-art global-scale Lagrangian three-dimensional chemistry-transport model (STOCHEM-CRI) is used to generate a comprehensive description of the atmospheric composition in the air traffic corridors in the upper troposphere and lower stratosphere. STOCHEM-CRI has been employed to describe the tropospheric distribution of ozone (Utembe et al., 2010) and of organic aerosol. STOCHEM-CRI has been employed to describe the tropospheric distribution of ozone (Utembe et al., 2010; Derwent et al., 2015) and of organic aerosol (Utembe et al., 2011). It has been used to explore different aspects of tropospheric chemistry involving formaldehyde (Cooke et al., 2010), peroxynitric acid (Bacak et al., 2011), the ozonolysis of ethene (Leather et al., 2012), Criegee intermediates (Percival et al., 2013), methanol (Khan et al., 2014), organic peroxy radicals (Khan et al., 2015a), organic hydroperoxides (2015b), acetone (Khan et al., 2015c), nitrate radicals (Khan et al., 2015d), alkyl nitrates (Khan et al., 2015e), dimethyl sulphide (Khan et al., 2016), peroxyacetyl nitrate (Khan et al., 2017a) and sesquiterpenes (Khan et al., 2017b). These studies each include a comprehensive comparison between observations and the predictions from STOCHEM-CRI.

STOCHEM-CRI has also been used to evaluate the impact of global aircraft NO_x emissions on atmospheric composition (Wasiuk et al., 2016a). An operational mitigation strategy for commercial aircraft impact on air quality and climate referred to as the turboprop replacement strategy (TRS) in which jets on short-haul missions were replaced with turboprops was investigated by the STOCHEM-CRI model (Wasiuk et al., 2016b). In a recent study, STOCHEM-CRI was used to assess the NO_x related climate impact of a switch from kerosene fuel to hydrogen fuel in the modelled aircraft (Khan et al., 2022).

The STOchastic CHEMistry (STOCHEM) model was initially developed to describe the global distributions of O_3, NO_x and CH_4. A detailed description of the model together with its horizontal and vertical coordinates, advection scheme and meteorological parameterisations and datasets is given in Collins et al., (1997). It has taken part in a number of global model intercomparisons and has performed satisfactorily in each (see, for example, Fiore et al., 2009: Naik et al., 2013; Stevenson et al., 2013; Young et al., 2013). This early version is called STOCHEM-OC. Subsequently in Utembe et al., (2011), the representation of the atmospheric chemistry of O_3, NO_x, carbon monoxide (CO), CH_4 and a range of organic compounds has been expanded considerably by incorporating the Common Representative Intermediate (CRI) chemical mechanism (Jenkin et al., 2008) and this newer version is called STOCHEM-CRI. Use of this enhanced version in combination with the box

model is particularly important for the accurate global representation O_3 formation from the photochemical oxidation of methane and other organic compounds under the low-NO_x conditions of the upper troposphere and lower stratosphere (Derwent et al., 2021).

In this study, STOCHEM-CRI was employed to generate background environmental conditions in the intercontinental air traffic corridors. STOCHEM-CRI was run with no aircraft NO_x emissions as input, whilst retaining NO_x emissions from lightning, stratospheric exchange, anthropogenic and soils. Results from a sensitivity case 'with aircraft' emissions are described in the Supplementary Information. STOCHEM-CRI model output was provided as background conditions appropriate to each latitude, longitude and altitude of each flight path location. These background conditions were set for the main tropospheric trace gases: CH_4, CO, H_2, O_3, NO_x=NO+NO_2, HNO_3, seven VOCs (ethane, propane, butane, ethylene, propylene, formaldehyde, acetaldehyde), CH_3OOH, and two peroxyacylnitrates.

2.4 Photochemical box model

The formulation of the box model was based on the Photochemical Trajectory Model (PTM), the details of which are given elsewhere (Derwent et al., 2010). The model follows the chemical development of O_3, NO_x, CH_4, CO and 7 organic compounds (ethane, propane, butane, ethylene, propylene, formaldehyde, acetaldehyde) within an air parcel for five days. The box model employs a near-explicit chemical mechanism based on the Master Chemical Mechanism v3.3.1 (Jenkin et al., 2015) taken from https://mcm.york.ac.uk.

The rate of change of the concentration of a chemical species, c_i, in molecule cm^{-3} within the air parcel was described by a series of differential equations of the form in equation (6):

$$dc_i/dt = P_i - L_i c_i \qquad (6),$$

where P_i is the instantaneous production rate of species, i, from chemistry and $L_i c_i$ is the instantaneous loss rate of species, i, from chemistry. The system of up to five thousand simultaneous stiff differential equations was integrated with a variable order Gear's method (FACSIMILE, Curtis and Sweetenham, 1987).

The box model was run for each of the 235 locations on 21 flight paths and was initialised with background environmental data for 36 species taken from STOCHEM-CRI as detailed above. Each box model was then run for five days beginning at 18:00 hours (UTC) on the first day. The start time was chosen so as to include a complete night-time during spin-up. The model run time was set at 5 days, long enough to include processes that return NO_y to NO_x but not too long as to move out of the linear regime. The photochemical O_3 production rate was calculated from the O_3 mixing ratios at the end and start of the five-day calculations. Mixing ratios of photochemically-generated reaction products such as HNO_3, H_2O_2 and HCHO were estimated from the box model results for midday on the second-day, the time of their maximum mixing ratios.

2.5 NO_x- and VOC-sensitivity indicator species and their ratios in the main intercontinental air traffic corridors

We began the analysis of the atmospheric chemistry regimes in the main intercontinental air traffic corridors in the UTLS region by focussing on twenty-one intercontinental flight paths during the spring season. The locations of the flight paths were noted at hourly intervals and atmospheric composition data from STOCHEM-CRI were employed as

background environmental conditions for the photochemical box modelling. A five-day box model run was performed for each of the 235 hourly flight path locations along the twenty-one flight paths to generate detailed atmospheric composition data for trace gases, reactive intermediates and free radicals with which to characterise the atmospheric chemistry regimes in the intercontinental air traffic corridors.

The photochemical box model was initialised using STOCHEM-CRI model output appropriate to mid-April at each latitude, longitude and altitude of each flight path. These initial conditions were set for the main tropospheric trace gases: CH_4, CO, H_2, O_3, NO_x=NO+NO_2, HNO_3, seven VOCs (ethane, propane, butane, ethylene, propylene, formaldehyde, acetaldehyde), CH_3OOH, and two peroxyacylnitrates. The five-day photochemical box model was then used to generate PO_3 values, OH, HO_2 and CH_3O_2 free radical number densities and mixing ratios of reaction products species such as H_2O_2, HCHO and PANs for each of the 235 flight path locations.

The first indicator of the atmospheric chemistry regime evaluated was the photochemical O_3 production rate (PO_3) over the five-day box model integration, calculated from the starting and ending O_3 mixing ratios. In the base case, the PO_3^{base}, averaged -0.24 ppb O_3 per 5 days over the 235 flight path locations, with a range from -0.62 to +0.45 ppb O_3 per 5 days. Overall, 206 locations showed net O_3 loss over the 5 days, with the remainder showing net O_3 production.

Two sensitivity cases were then performed at each location: in one, the initial NO_x and NO_z mixing ratios were decreased by 30% and, in the other, the VOC mixing ratios were decreased by 30%. These are the NO_x-control and VOC-control sensitivity cases, respectively. In the NO_x-control scenario case, the photochemical O_3 production rates, PO_3^{nox}, decreased relative to PO_3^{base} at all of the 235 flight path locations. The NO_x responses, $\Delta PO_3^{nox} = PO_3^{base} - PO_3^{nox}$, averaged 0.12 ppb O_3 per 5 days, covering a range from 0.02 to 0.55 ppb O_3 per 5 days. In the VOC-control scenario case, again all the photochemical O_3 productions rates, PO_3^{voc}, decreased relative to PO_3^{base} at all locations. The VOC responses, $\Delta PO_3^{voc} = PO_3^{base} - PO_3^{voc}$, averaged 0.12 ppb O_3 per 5 days and covered a range from 0.05 to 0.35 ppb O_3 per 5 days.

As in the polluted atmospheric boundary layer, the issue was whether the O_3 responses to the 30% NO_x controls were greater than or less than the O_3 responses to the 30% VOC controls at each flight path location. If the O_3 response to the NO_x control was greater than the response to the VOC control, then the atmospheric chemistry regime is said to be NO_x-sensitive or NO_x-limited. However, if the O_3 responses to the NO_x control was less than the response to the VOC control, then the atmospheric chemistry regime is said to be VOC-sensitive or VOC-limited. Out of the 235 flight path locations, 90 were classed as NO_x-sensitive, 137 were classed as VOC-sensitive and 8 could not be classified because the NO_x- and VOC-responses were identical.

To more clearly delineate those locations within the different atmospheric chemistry regimes, a metric N – V was defined as: $N - V = \Delta PO_3^{nox} - \Delta PO_3^{voc}$, then positive values of N – V would represent NO_x-sensitivity and negative values represent VOC-sensitivity. Averaged over all flight path locations, the mean N – V for spring was found to be 0.0031 ± 0.1 (quoting 2 – σ confidence limits here and elsewhere below) ppb O_3 per 5 days. Broadly speaking, the longitude of the flight path location made little difference to the atmospheric

chemistry regime. There was a tendency for locations in the western hemisphere to be more VOC-sensitive than those in the eastern hemisphere, that is to say N – V was more negative, -0.02 ± 0.08 ppb O_3 per 5 days versus 0.02 ± 0.1 ppb O_3 per 5 days, respectively, but these differences were not statistically significant. There was a strong influence of latitude on atmospheric chemistry regime, with N – V being more positive at low latitudes and more negative at high latitudes.

The use of PO_3, as an indicator of atmospheric chemistry regime in the UTLS (Nussbaumer et al., 2023) is not without drawbacks and a number of other indicator species and their ratios have been proposed in the literature, including O_3/NO_z, $HCHO/NO_2$, H_2O_2/HNO_3 and α^{CH3O2}, as discussed above. These indicators and their ratios were estimated from box model output taken at midday on the second-day. To assess the applicability and specificity of the different indicator species ratios, scatter plots were employed of the indicator species ratios versus N – V at each flight path location. The aim is to ascertain if there is a sufficiently clear demarcation in the indicator species ratios between NO_x- and VOC-sensitivity.

A scatter plot of the four indicator ratios plotted out against N – V is presented in Figure 2. There was a demarcation between the NO_x-sensitive (N – V positive) and VOC-sensitive (N – V negative) locations, with O_3/NO_z ratios below 200 being the former and above 200 being the latter. An analogous demarcation was found for the $HCHO/NO_2$ indicator ratio with a demarcation at about $HCHO/NO_2$ = 7.5 between NO_x-sensitive and VOC-sensitive locations. There was also a demarcation at H_2O_2/HNO_3 = 6. The α^{CH3O2} indicator provided the clearest demarcation between NO_x-sensitive and VOC-sensitive regimes at α^{CH3O2} = 0.69, in confirmation of the analyses performed by Nussbaumer et al., (2023). The scatter plot in Figure 2 confirms that all five metrics: PO_3, O_3/NO_z, $HCHO/NO_2$, H_2O_2/HNO_3 and α^{CH3O2} generate a consistent and robust evaluation of the atmospheric chemistry regimes active in the intercontinental air traffic corridors in the UTLS region during the spring season. The CTM/box model approach has therefore provided a robust basis on which we can proceed to evaluate the impact of aviation NO_x emissions on O_3 in the UTLS region.

3. Quantifying the impact of NO_x on O_3 in the intercontinental air traffic corridors

Having identified that the rate of photochemical ozone formation (PO_3) provides an accurate and consistent indicator of atmospheric chemical regime by comparison with four other indicators, we can be confident that ΔPO_3^{nox} values can be used as a robust gauge of the impact of NO_x emissions from aviation on O_3 levels in the international air traffic corridors of the UTLS. The aim is to provide some insights into which locations within the intercontinental air traffic corridors are more likely to be strongly impacted by aircraft NO_x emissions and those which are likely to be much less impacted.

As a measure of the impact of NO_x on O_3, we define the $\partial O_3/\partial NO_x$ metric from the O_3 responses to the 30% reductions in NO_x and NO_y, ΔPO_3^{nox}, normalised by the NO_x reduction, ΔNO_x, as follows:

$$\partial O_3/\partial NO_x = \Delta PO_3^{nox}/ \Delta NO_x \quad (7).$$

The values of the $\partial O_3/\partial NO_x$ metric are presented in Figures 3a-d for each flight path location and each season. $\partial O_3/\partial NO_x$ values varied from 5.4 to 37.5 per ppb NO_x per 5 days (henceforward ppb ppb^{-1} per 5 days), with highest values towards low latitudes and lowest

values towards high latitudes. Metric values in these maps appeared highest during July and lowest during April.

Taking all 235 flight locations, all four seasons, we found a grand average for $\partial O_3/\partial NO_x$ of 22 ± 6 ppb ppb^{-1} per 5 days. Averaging the photochemical ozone production over the five days, this is equivalent to an O_3 productivity of about 4 – 5 molecules of O_3 produced per molecule of NO_x oxidised in the intercontinental air corridors of the UTLS.

Average $\partial O_3/\partial NO_x$ values over the 235 flight locations are tabulated in Table 2 and showed evidence of a seasonal variation. $\partial O_3/\partial NO_x$ peaked in the July at 26.4 ppb ppb^{-1} per 5 days, being slightly lower at 24.8 ppb ppb^{-1} per 5 days in October and reached a minimum in April at 15.7 ppb ppb^{-1} per 5 days. The January value of 22.7 ppb ppb^{-1} per 5 days was close to the annual average. Average $\partial O_3/\partial NO_x$ values showed a small difference between the western and eastern hemispheres, 22.0 versus 22.7 ppb ppb^{-1} per 5 days, respectively, but this was not likely to be statistically significant. Annual average $\partial O_3/\partial NO_x$ values exhibited a decreasing trend polewards. Low latitudes (below 45°N) averaged 30.8 ppb ppb^{-1} per 5 days, whilst mid-latitudes (45°N – 55°N) gave 22.5 ppb ppb^{-1} per 5 days. High latitudes (above 70°N) averaged only 9.4 ppb ppb^{-1} per 5 days during April.

Armed with this impact measure of NO_x upon O_3, we will begin to study how the impact of aviation NO_x emissions varies with season and location in the intercontinental air traffic corridors, with a view to assessing the likely effects of mitigation options. Since there was unlikely to be any significant variation of $\partial O_3/\partial NO_x$ with longitude, attention was initially focussed on variations of $\partial O_3/\partial NO_x$ with the latitudes of the 235 flight path locations in each season, see Figure 4. Figure 4 presents a scatter plot of $\partial O_3/\partial NO_x$ with latitude, with the different seasons plotted with different symbols. Latitudinal variations were apparent in all seasons, with a strong tendency for $\partial O_3/\partial NO_x$ to decrease polewards and increase towards low latitudes. Highest $\partial O_3/\partial NO_x$ were found below 40°N and lowest above 70°N. Highest $\partial O_3/\partial NO_x$ were found during summer and autumn and lowest during spring. Annual averages varied by about a factor of two between low and high latitudes, whilst maxima and minima $\partial O_3/\partial NO_x$ showed a factor of seven variation.

Whilst variations of $\partial O_3/\partial NO_x$ with longitude generally exhibited a significant amount of scatter and small differences between the hemispheres, the longitudinal distribution of $\partial O_3/\partial NO_x$ is worthy of some comment, see Figure 5. Figure 5 presents a scatter plot of $\partial O_3/\partial NO_x$ versus longitude for autumn (shown as black plus signs) overlaid with the corresponding spring, summer, winter and annual data averaged over 30° longitude bins. Whilst there is considerable scatter in the 235 autumn data points, a series of low $\partial O_3/\partial NO_x$ points is apparent between 0° and 10° E. The average $\partial O_3/\partial NO_x$ over 0° – 100°E was found to be 18.3 ppb ppb^{-1} per 5 days, compared with 26.8 ppb ppb^{-1} per 5 days elsewhere. The lowest point with $\partial O_3/\partial NO_x$ = 10.7 ppb ppb^{-1} per 5 days was found at (23.86°E, 57.92°N) over the Baltic region on a great-circle flight from London, UK to Peking, China. The maximum point with $\partial O_3/\partial NO_x$ = 37.5 ppb ppb^{-1} per 5 days was found at (101.81°E, 29.8°N) over China on great-circle flights from Paris, France and Munich, Germany to Hong Kong, China. These maxima and minima serve to reinforce the general trend with $\partial O_3/\partial NO_x$ decreasing polewards and increasing towards lower latitudes.

To aid the exploration of the geographical variations in the NO_x – O_3 impact metric $\partial O_3/\partial NO_x$, Table 2 presents the averages over 30° longitude x 10° latitude cells for each

season. The 235 flight path locations are distributed over 40 cells, with significant variations in occupancy, as dictated by our choice of intercontinental flight departures and arrivals. In winter, the impact metric varied from 19 to 35 ppb ppb^{-1} per 5 days, with an average of 22.2 ppb ppb^{-1} per 5 days. The maximum impact metric occurred over southern China and was found to be about 60% higher than the seasonal average. This location is associated with the intercontinental flight paths from Europe to Asia. In spring, the impact metric varied from 6 to 29 ppb ppb^{-1} per 5 days, with an average of 14.8 ppb ppb^{-1} per 5 days, significantly lower than the winter seasonal average. The maximum occurred over southern China, again, as in the winter season but a factor of two higher than the spring season average.

The summer values of the impact metric varied from 17 to 33 ppb ppb^{-1} per 5 days, with an average of 26.0 ppb ppb^{-1} per 5 days, the highest of all four seasons. The maximum metric was found over northern China, south east Russia, a location associated with intercontinental flights from North America to Asia. The impact metric varied from 17 to 35 ppb ppb^{-1} per 5 days during autumn, with an average of 25.4 ppb ppb^{-1} per 5 days. The maximum impact metric was found over central China, some 40% higher than the seasonal average, associated with intercontinental flight paths from Europe to Asia.

A notable feature of the impacts of NO_x upon O_3 in the intercontinental air traffic corridors is that the impact metrics are not spatially invariant, indeed they are highly spatially variable. The spatial variability of the impact metrics implies that there is a highly non-linear relationship between O_3 and NO_x. This non-linearity is more pronounced at low-NO_x levels. We can illustrate this non-linearity by plotting out the NO_x – O_3 impact metrics versus background NO_x for spring in the intercontinental air traffic corridors as shown in Figure 6. The impact of the non-linear chemistry is most noticeable at low-NO_x levels. A consequence of this non-linearity is that care must be taken in setting up the background environmental conditions for CTM/box model calculations, hence our use of 'no aircraft' emissions.

In summary, we have employed a robust NO_x – O_3 impact metric to explore locations within the intercontinental air traffic corridors that are likely to be more or less strongly impacted by aircraft NO_x emissions. O_3 levels in the region bounded by 20 – 50^{o}N and 90 – 150^{o}E, over Asia, are much more strongly impacted by NO_x compared to air traffic corridor averages. These impacts could be up to a factor of two stronger compared to air traffic corridor averages. Trans-polar routes are associated with regions where the NO_x – O_3 impact metrics are over a factor of two lower than air traffic corridor averages.

4. Discussion and conclusions

This study, a CTM/box model approach has been employed to quantify the ozone versus NO_x sensitivity in air traffic corridors over time-scales of hours and over distance scales appropriate to aircraft flight paths. An important feature of this study is the marked contrast that the CTM/box model approach offers over the global CTM models currently used to assess the impacts of aviation NO_x on ozone and their mitigation options. We show how the concepts of NO_x-sensitive and VOC-sensitive can be applied successfully in the air traffic corridors through detailed comparisons with indicator species ratios such as: O_3/NO_z, $HCHO/NO_2$, H_2O_2/HNO_3 and α^{CH3O2}. By this means, we are able to demonstrate that the impact of NO_x on the rate of photochemical ozone production in the box model is likely to be a robust indicator of the impact of aircraft NO_x on O_3 levels in the air traffic corridors of the UTLS. To this end, an impact metric $\partial O_3/\partial NO_x$ has been defined for use in identifying

those locations in the air traffic corridors that are more and less likely to be impacted by aircraft NO_x emissions.

Taking all 235 flight locations, all four seasons, we found an average photochemical ozone production that was equivalent to an O_3 productivity of about 4 – 5 molecules of O_3 produced per molecule of NO_x oxidised in the intercontinental air corridors of the UTLS. This O_3 productivity is exactly similar to that found on the urban and regional scales in the European polluted boundary layer where the productivity was found to be between 4 – 6 molecules per molecule (Derwent and Davies, 1994). Our study is also comparable to the study of Song et al. (2022) who showed 1-6 molecules of O_3 production for each NO_x molecule oxidized at a polluted city in China, Guangdong. O_3 productivities in the range of 2 – 12 have been reported in US studies as reviewed by Zaveri et al., (2003), who reported a productivity of 4.7 ± 0.2 in the Southern Oxidant Study, in excellent agreement with our findings.

The O_3 versus NO_x sensitivities found here with the CTM/box model approach appear to be significantly smaller than reported in global CTM studies of aviation impacts and their mitigation. For example, Stevenson and Derwent (2009) find OPEs of between 6 and 24 O_3 molecules per NO_x molecule whilst Dahlmann et al. (2011) report an efficiency of 50 O_3 molecules per NO_x molecules for aviation. Lee et al., (2010) (in their Figure 13) report globally integrated OPEs in the range 13 – 42 from seven early literature studies of the global impacts of aircraft NO_x emissions. These ozone productivities from global CTM studies are up to 10 times higher than we have found here with the CTM/box model approach. In addition to the OPEs, Lee et al., (2010) also report the short-term radiative forcing from the additional O_3 as 36.9 mWm^{-2} /Tg N yr^{-1} from the same seven early studies. Sovde et al., 2014 reviewed three CTM and two climate-chemistry models and reported a short-term radiative forcing of 27.4 mWm^{-2} / Tg N yr^{-1}. Recent reviews quote 36.0 mWm^{-2} /Tg N yr^{-1} (Lee et al., 2021), so it appears that more recent global CTM studies are also showing similar elevated OPEs.

It is concluded that this contrast is likely to be due in part to the larger spatial scale of the global CTMs which leads to the spreading of the aviation NO_x emissions over 100s of kilometres and maintains NO_x emissions over timescales of a month, an order of magnitude longer than the CTM/box model approach used here. This conclusion supports the findings of Lee et al., (2023) that coarse resolution global CTMs have overestimated aviation's impacts on air quality because they are unable to resolve local-scale effects.

Average $\partial O_3/\partial NO_x$ values over the 235 flight locations showed evidence of a seasonal variation. $\partial O_3/\partial NO_x$ peaked in the summer season, was slightly lower in autumn and reached a minimum in spring. The winter O_3 productivity was close to the annual average. The peak solar flux is located at about 20°N during summer and thus the photochemistry due to more incoming solar radiation between 30°N and 60°N covering 235 flight locations during summer is more rapid resulting in higher ozone production than that during other seasons. Our study showed the summer values of the impact metric is higher at midlatitudes (40°N-60°N) compared with lower latitudes (<40°N), which is consistent with Maruhashi et al. (2022) and Gauss et al. (2006). The winter O_3 production in our study was smaller than that found by Maruhashi et al. (2022) and Frömming et al. (2021). In our study, the winter low latitudes showed the highest O_3 productivities relative to mid-latitudes. Similar trends are seen for autumn and spring. The latitudinal variations for different seasons in our study

are found to be consistent with Maruhashi et al. (2022), Frömming et al. (2021), Rosanka et al. (2020), Stevenson and Derwent (2009), Köhler et al. (2008), Köhler et al. (2013), Grewe and Stenke (2008), Berntsen et al. (2005) studies.

It is further concluded that the widening of the spatial scales and extension of timescales found in global CTM studies does not appear to have inadvertently hidden the geographical variations found here with the CTM/box model approach, with O_3 versus NO_x sensitivities appearing largest in low latitudes and smallest in high latitudes. We have shown that NO_x impacts are significantly smaller and but not distributed differently across northern midlatitudes, as a result of the different time and distance scales employed in the CTM/box model approach. Trans-polar routes are associated with regions that are much less strongly impacted by NO_x as the low latitude routes into Asia. Further research will be required to confirm our assessment of those air traffic corridors that appear to show greatest NO_x – O_3 impacts and those the least. Consideration should be given to a metric or measure which considers NO_x – O_3 climate impacts. The climate-optimal aircraft routing may have the potential for a drastic climate impact reduction in a relatively short time-frame, whilst requiring minimal technology changes to the current fleet and ground information.

Acknowledgements

MAHK thanks the University of Bristol Climate and Net Zero Impact Award under whose auspices various aspects of this work were supported. MD was funded through an EPSRC summer internship. We thank Mr Kieran Tait for his valuable support to extract the flight trajectory from OpenSky data network.

References

Bacak, A., Cooke, M.C., Bardwell, M.W., McGillen, M.R., Archibald, A.T., Huey, L.G., Tanner, D., Utembe, S.R., Jenkin, M.E., Derwent, R.G., Shallcross, D.E., Percival, C.J., 2011. Kinetics of the HO_2 + NO_2 reaction: On the impact of new gas-phase kinetic data for the formation of HO_2NO_2 on HO_x, NO_x and HO_2NO_2 levels in the troposphere. Atmospheric Environment 45, 6414-6422.

Berntsen, T., Fuglestvedt, J., Joshi, M., Shine, K., Stuber, N., Ponater, M., Sausen, R., Hauglustaine, D., and Li, L., 2005. Response of climate to regional emissions of ozone precursors: sensitivities and warming potentials. Tellus B 57, 283–304.

Carslaw, K.S., Lee, L.A., Regayre, L.A., Johnson, J.S., 2018. Climate Models are uncertain, but we can do something about it. Earth&Space News 15-16 EOS.org.

Chameides, W.L., Walker, J.C.G., 1973. A photochemical theory for tropospheric ozone. Journal of Geophysical Research 78, 8751-8760.

Collins, W.J., Stevenson, D.S., Johnson, C.E., Derwent, R.G., 1997. Tropospheric ozone in a global-Scale three-dimensional Lagrangian model and its response to NO_x emission controls. Journal of Atmospheric Chemistry 26, 223-274.

Cooke, M.C., Utembe, S.R., Carbajo, P.C., Archibald, A.T., Orr-Ewing, A.J., Jenkin, M.E., Derwent, R.G., Lary, D.J., Shallcross, D.E., 2010. Impacts of formaldehyde photolysis rates on tropospheric chemistry. Atmospheric Sciences Letters 11, 33-38.

Crutzen, P.J., 1973. Photochemical reactions initiated by and influencing ozone in the unpolluted troposphere. Tellus 26, 47-57.

Curtis, A.R., Sweetenham, W.P., 1987. FACSIMILE release H user's manual. AERE Report R11771, HMSO London.

Dahlmann, K., Grewe, Ponater, S., Matthes, S., 2011. Quantifying the contributions of individual NO_x sources to the trend in ozone radiative forcing. Atmospheric Environment 45, 2860–2868.

Derwent, R.G., Davies, T.J., 1994. Modelling the impact of NO_x or hydrocarbon control on photochemical ozone in Europe. Atmospheric Environment 28, 2039-2052.

Derwent, R.G., Witham, C.S., Utembe, S.R., Jenkin, M.E., Passant, N.R., 2010. Ozone in Central England: The impact of 20 years of precursor emission controls in Europe. Environmental Science and Policy 13, 195-204.

Derwent, R.G,, Utembe, S.R., Jenkin, M.E., Shallcross, D.E., 2015. Tropospheric ozone production regions and the intercontinental origins of surface ozone over Europe. Atmospheric Environment 112, 216-224.

Derwent, R.G., Stevenson, D.S., Utembe, S.R., Jenkin, M.E., Khan, A.H., Shallcross, D.E., 2020. Global modelling studies of hydrogen and its isotopomers using STOCHEM-CRI: Likely radiative forcing consequences of a future hydrogen economy. International Journal of Hydrogen Energy 45, 9211-9221.

Derwent, R.G., et al., 2021. Intercomparison of the representations of the atmospheric chemistry of pre-industrial methane and ozone in earth system and other global chemistry-transport models. Atmospheric Environment 248, 118248.

Derwent, R.G., Utembe, S.R., Jenkin, M.E., Khan, M.A.H., Shallcross, D.E., 2023. Investigating the role of organic compounds in intercontinental ozone transport: Reactivity scales and Global warming Potentials. Atmospheric Environment 306, 119817.

Fiore, A.M., et al., 2009. Multimodel estimates of intercontinental source-receptor relationships for ozone pollution. Journal of Geophysical Research 114, D043041.

Frömming, C., Grewe, V., Brinkop, S., Jöckel, P., Haslerud, A.S., Rosanka, S., van Manen J., Matthes, S., 2021. Influence of weather situation on non-CO2 aviation climate effects: the REACT4C climate change functions. Atmospheric Chemistry and Physics 21, 9151–9172.

Gauss, M., Isaksen, I. S. A., Lee, D. S., and Søvde, O. A., 2006. Impact of aircraft NO_x emissions on the atmosphere – tradeoffs to reduce the impact. Atmospheric Chemistry and Physics 6, 1529–1548.

Grewe, V. and Stenke, A., 2008. AirClim: an efficient tool for climate evaluation of aircraft technology. Atmospheric Chemistry and Physics 8, 4621–4639.

IATA, 2023. Our commitment to fly net zero. International Air Transport Association, Montreal, Canada. https://www.iata.org/en/programs/environment/flynetzero/

IPCC, 2018. Climate Change 2013: The Physical Science Basis. Appendix 8.A, Cambridge University Press, Cambridge, UK.

Jaegle, L., Jacob, D.J., Brune, W., Tan, D., Faloona, I., Weinheimer, A., Ridley, B., Campos, T., Sachse, G., 1998. Source of HO_x and production of ozone in the upper troposphere over the United States. Geophysical Research Letters 25, 1709-1712.

Jenkin, M.E., Watson, L.A., Utembe, S.R., Shallcross, D.E., 2008. A Common Representative Intermediates (CRI) mechanism for VOC degradation. Part 1: Gas phase mechanism development. Atmospheric Environment 42, 7185-7195.

Jenkin, M.E., Young, J.C., and Rickard, A.R., 2015. The MCM v3.3.1 degradation scheme for isoprene. Atmospheric Chemistry and Physics 15, 11433-11459.

Khan, M.A.H., Cooke, M.C., Utembe, S.R., Xiao, P., Derwent, R.G., Jenkin, M.E., Archibald, A.T., Maxwell, P., Morris, W.C., South, N., Percival, C.J., Shallcross, D.E., 2014. Reassessing the photochemical production of methanol from peroxy radical self and cross reactions using the STOCHEM-CRI global chemistry and transport model. Atmospheric Environment 99, 77-84.

Khan, M.A.H., Cooke, M.C., Utembe, S.R., Archibald, A.T., Derwent, R.G., Jenkin, M.E., Morris, W.C., South, N., Hansen, J.C., Francisco, J.S., Percival, C.J., Shallcross, D.E., 2015a. Global analysis of peroxy radicals and peroxy radical-water complexation using the STOCHEM-CRI global chemistry and transport model. Atmospheric Environment 106, 278-287.

Khan, M.A.H., Cooke, M.C., Utembe, S.R., Xiao, P., Morris, W.C., Derwent, R.G., Archibald, A.T., Jenkin, M.E., Percival, C.J., Shallcross, D.E., 2015b. The global budgets of organic hydroperoxides for present and pre-industrial scenarios. Atmospheric Environment 110, 65-74.

Khan, M.A.H., Cooke, M.C., Utembe, S.R., Archibald, A.T., Maxwell, P., Morris, W.C., Xiao, P., Derwent, R.G., Jenkin, M.E., Percival, C.J., Walsh, R.C., Young, T.D.S., Simmonds, P.G., Nickless, G., O'Doherty, S., Shallcross, D.E., 2015c.The global atmospheric budget and distribution of acetone using the 3-D global model, STOCHEM-CRI. Atmospheric Environment 112, 269-277.

Khan, M.A.H, Cooke, M.C., Utembe, S.R., Archibald, A.T., Derwent, R.G., Xiao, P., Percival, C.J., Jenkin, M.E., Morris, W.C., Shallcross, D.E., 2015d. Global modelling of the nitrate radical (NO_3) for present and pre-industrial scenarios. Atmospheric Research 164-165, 347-357.

Khan, M.A.H., Cooke, M.C., Utembe, S.R., Morris, W.C., Archibald, A.T., Derwent, R.G., Jenkin, M.E., Orr-Ewing, A.J., Higgins, C.M., Percival, C.J., Leather, K.E., Shallcross, D.E., 2015e. Global modelling of the $C_1 – C_3$ alkyl nitrates using STOCHEM-CRI. Atmospheric Environment 123, 256-267.

Khan, M.A.K., Gillespie, S.M.P., Razis, B., Xiao, P., Davies-Coleman, M.T., Percival, C.J., Derwent, R.G., Dyke, J.M., Ghosh, M.V., Lee, E.P.F., Shallcross, D.E., 2016. A modelling study of the atmospheric chemistry of DMS using the global model STOCHEM-CRI. Atmospheric Environment 127, 69-79.

Khan, M.A.H., Cooke, M.C., Utembe, S.R., Archibald, A.T., Derwent, R.G., Jenkin, M.E., Leather, K.E., Percival, C.J., Shallcross, D.E., 2017a. Global budget and distribution of peroxyacetyl nitrate (PAN) for present and pre-industrial scenarios. International Journal of Earth and Environmental Science 2, 130-140.

Khan, M.A.H., Jenkin, M.E., Foulds, A., Derwent, R.G., Percival, C.J., Shallcross, D.E., 2017b. A modelling study of secondary organic aerosol formation from sesquiterpenes using the STOCHEM global chemistry and transport model. Journal of Geophysical Research 122, doi:10.1002/2016JD026415.

Khan, M.A.H., Brierley, J., Tait, K.N., Bullock, S., Shallcross, D.E., Lowenberg, M.H., 2022. The emissions of water vapour and NO_x from modelled hydrogen-fuelled aircraft and the impact of NO_x reduction on climate compared with kerosene-fuelled aircraft. Atmosphere 13, 1660.

Khan, M.A.H., Tait, K., Derwent, R.G., Roome, S., Bacak, A., Bullock, S., Lowenberg, M.H., Shallcross, D.E., 2023. Off-setting climate change through formation flying of aircraft, a feasibility study reliant on high fidelity gas-phase chemical kinetic data. International Journal of Chemical Kinetics 55, 402-412. DOI: 10.1002/kin.21644.

Köhler, M., Radel, G., Dessens, O., Shine, K., Rogers, H., Wild, O., and Pyle, J., 2008. Impact of perturbations to nitrogen oxide emissions from global aviation. Journal of Geophysical Research-Atmospheres 113, D11305.

Köhler, M. O., Rädel, G., Shine, K. P., Rogers, H. L., and Pyle, J. A., 2013. Latitudinal variation of the effect of aviation NO_x emissions on atmospheric ozone and methane and related climate metrics. Atmospheric Environment 64, 1–9.

Leather, K.E., McGillen, M.R., Cooke, M.C., Utembe, S.R., Archibald, A.T., Jenkin, M.E., Derwent, R.G., Shallcross, D.E., 2012. Acid-yield measurements of the gas-phase ozonolysis of ethene as a function of humidity using chemical ionisation mass spectrometry. Atmospheric Chemistry and Physics 12, 469-479.

Lee, D.S., Pitari, G., Grewe, V., Gierens, K., Penner, J.E., Petzold, A., Prather, M.J., Schumann, U., Bais, A., Berntsen, T., Iachetti, D., Lim, L.L., Sausen, R., 2010. Transport impacts on atmosphere and climate: Aviation. Atmospheric Environment 44, 4678–4734.

Lee, D.S., Fahey, D.W., Skowron, A., Allen, M.R., Burkhardt, U., Chen, Q., Doherty, S.J., Freeman, S., Forster, P.M., Fuglestvedt, J., Gettelman, A., De Leon, R.R., Lim, L.L., Lund, M.T., Millar, R.J., Owen, B., Penner, J.E., Pitari, G., Prather, M.J., Sausen, R., Wilcox, L.J., 2021. The contribution of global aviation to anthropogenic climate forcing for 2000 to 2018. Atmospheric Environment 244, 117834.

Lee, D.S., Allen, M.R., Cumpsty, N., Owen, B., Shine, K.P., Skowron, A., 2023. Uncertainties in mitigating aviation non-CO_2 emissions for climate and air quality using hydrocarbon fuels. Environmental Science: Atmospheres, DOI: 10.1039/d3ea00091e.

Maruhashi, J., Grewe, V., Frömming, C., Jöckel, P., Dedoussi, I.C., 2022. Transport patterns of global aviation NO_x and their short-term O_3 radiation forcing-a machine learning approach. Atmospheric Chemistry and Physics 22, 14253–14282.

Naik, V., et al. (2013). Pre-industrial to present-day changes in tropospheric hydroxyl and methane lifetime from the Atmospheric Chemistry and Climate Model Intercomparison Project (ACCMIP). Atmospheric Chemistry and Physics 13, 5277-5298.

Nussbaumer, C.M., Fischer, H., Lelieveld, J. Pozzer, A., 2023. What controls ozone sensitivity in the upper troposphere? EGUsphere https://doi.org/10.5194/egusphere-2023-816.

Percival, C.J., Welz, O., Eskola, A.J., Savee, J.D., Osborn, D.L., Topping, D.O., Lowe, D., Utembe, S.R., Bacak, A., McFiggans, G., Cooke, M.C, Xiao, P., Archibald, A.T., Jenkin, M.E., Derwent, R.G., Riipinen, I., Mok, D.W.K., Lee, E.P.F., Dyke, J.M., Taatjes, C.A., Shallcross, D.E., 2013. Regional and global impacts of Criegee intermediates on atmospheric sulphuric acid concentrations and first steps of aerosol formation. Faraday Discussions of the Chemical Society 105, 45-73. DOI: 10.1039/c3fd00048f.

Rosanka, S., Frömming, C., and Grewe, V., 2020. The impact of weather patterns and related transport processes on aviation's contribution to ozone and methane concentrations from NOx emissions, Atmospheric Chemistry and Physics 20, 12347–12361.

Sillman, S., 1995. The use of NO_y, H_2O_2 and HNO_3 as indicators for ozone-NO_x-hydrocarbon sensitivity in urban locations. Journal of Geophysical Research Atmospheres 100, 14175-14188.

Sillman, S., 1999. The relation between ozone, NOx and hydrocarbons in urban and polluted environments. Atmospheric Environment 33, 1821-1845.

Sillman, S., Logan, J.A., Wofsy, S.C., 1990. The sensitivity of ozone to nitrogen oxides and hydrocarbons in regional ozone episodes. Journal of Geophysical Research 95, 1837-1851.

Song, K., Liu, R., Wang, Y., Liu, T., Wei, L., Wu, Y., Zheng, J., Wang, B., Liu, S.C., 2022. Observation-based analysis of ozone production sensitivity for two persistent ozone episodes in Guangdong, China. Atmospheric Chemistry and Physics 22, 8403-8416.

Søvde, O.A., Matthes, S., Skowron, A., Iachetti, D., Lim, L., Bethan, O., Hodnebrog, Ø, Genova, G.D., Pitari, G., Lee, D.S., Myhre, G., Isaksen, I.S.A., 2014. Aircraft emission mitigation by changing route altitude: A multi-model estimate of aircraft NOx emission impact on O3 photochemistry. Atmospheric Environment 95, 468-479.

Stevenson, D.S., Derwent, R.G., 2009. Does the location of aircraft NO_x emissions affect their climate impact. Geophysical Research Letters 36, L17180.

Stevenson, D.S., et al., 2013. Tropospheric ozone changes, radiative forcing and attribution to emissions in the Atmospheric Chemistry and Climate Model Intercomparison Project (ACCMIP). Atmospheric Chemistry and Physics 13, 3063-3085.

Transport & Environment, 2018. Roadmap to decarbonising European aviation. European Federation for Transport and Environment, Brussels, Belgium. https://transportenvironment.org/discover/roadmap-decarbonising-european-aviation/

Transport & Environment, 2023. The cost of hydrogen aviation. European Federation for Transport and Environment, Brussels, Belgium. https://www.transportenvironment.org/wp-content/uploads/2023/05/The-cost-of-hydrogen-aviation-Final-Briefing-2.pdf

Utembe, S.R., Cooke, M.C., Archibald, A.T., Jenkin, M.E., Derwent, R.G., Shallcross, D.E., 2010. Using a reduced Common Representative Intermediates (CRI v2-R5) mechanism to simulate tropospheric ozone in a 3-D Lagrangian chemistry transport model. Atmospheric Environment 13, 1609-1622.

Utembe, S.R., Cooke, M.C., Archibald, A.T., Shallcross, D.E., Derwent, R.G., Jenkin, M.E., 2011. Simulating secondary organic aerosol in a 3-D Lagrangian chemistry transport model

using the reduced Common Representative Intermediate mechanism (CRI v2-R5). Atmospheric Environment 45, 1604-1614.

Wasiuk, D.K., Khan, M.A.H., Shallcross, D.E., Lowenberg, M.H., 2016a. The impact of global aviation NO_x emissions on tropospheric composition changes from 2005 to 2011. Atmospheric Research 178-179, 73-83.

Wasiuk, D.K., Khan, M.A.H., Shallcross, D.E., Derwent, R.G., Lowenberg, M.H., 2016b. A mitigation strategy for commercial aviation impact on NO_x-related O_3 change. Journal of Geophysical Research Atmosphere 121, 8730-8740.

Wild, O., Prather, M.J., 2000. Excitation of the primary tropospheric chemical mode in a global three-dimensional model. Journal of Geophysical Research 105, 24,647-24,660.

Wild, O., Prather, M.J., Akimoto, H., 2001. Indirect long-term global radiative cooling from NO_x emissions. Geophysical Research Letters 28, 1719-1722.

Young, P. J., et al. (2013). Pre-industrial to end 21st century projections of tropospheric ozone from the Atmospheric Chemistry and Climate Model Intercomparison Project. Atmospheric Chemistry and Physics 13, 2063-2090.

Zaveri, R.A., Berkowitz, C.M., Kleinmann, L.I., Springston, S.R., Doskey, P.V., Lonnemann, W.A., Spicer, C.W., 2003. Ozone production efficiency and NO_x depletion in an urban plume: Interpretation of field observations and implications for evaluating O_3 – NO_x – VOC sensitivity. Journal of Geophysical Research 108, D14, 4436, doi:10.1029/2002JD003144.

Table 1. Details of the 21 flight paths studied, giving flight lengths, start and end locations and three-letter airport codes.

No.	Route	Flight length, hours	Flight start and end locations, airport codes
1	CDG-JFK	10	Paris (CDG) – New York (JFK)
2	PEK-MUC	10	Beijing (PEK) – Munich (MUC)
3	HKG-JFK	16	Hong Kong (HKG) – New York
4	PEK-JFK	14	Beijing – New York
5	CDG-HKG	12	Paris – Hong Kong
6	CDG-PEK	11	Paris - Beijing
7	CDG-SFO	11	Paris – San Francisco (SFO)
8	HKG-JFK	16	Hong Kong – New York
9	PEK-LHR	11	Beijing – London (LHR)
10	PEK-YVR	11	Beijing – Vancouver (YVR)
11	SFO-PEK	12	San Francisco – Beijing
12	HKG-LHR	12	Hong Kong – London
13	HKG-MUC	11	Hong Kong - Munich
14	HKG-SFO	14	Hong Kong – San Francisco
15	HKG-YVR	13	Hong Kong – Vancouver
16	LHR-JFK	8	London – New York
17	LHR-SFO	11	London – San Francisco
18	LHR-YVR	10	London – Vancouver
19	MUC-JFK	9	Munich – New York
20	MUC-SFO	12	Munich – San Francisco
21	MUC-YVR	11	Munich – Vancouver

Table 2. NO_x – O_3 impact metric $\partial O_3/\partial NO_x$ averaged over each 30° longitude and 10° latitude cell during each season in the intercontinental air traffic corridors.

Latitude range, °N	180 – 150°W	150 – 120°W	120 – 90°W	90 – 60°W	60 – 30°W	30 – 0°W	30 – 60°E	60 – 90°E	90 – 120°E	120 – 150°E	150 – 180oE
Winter											
80 – 90°N		19	19							20	19
70 – 80°N			19	19	22	22				21	
60 – 70°N	21	22	22	20	22	23	24	22	21	22	22
50 – 60°N	20	23	23	21	22	24	22	22	22	20	20
40 – 50°N		25	24	21				26	23	19	
30 – 40°N									31	22	
20 – 30°N									35		
Spring											
80 – 90°N		8	10							6	8
70 – 80°N			10	8	13	13				9	
60 – 70°N	11	8	11	10	17	15	14	10	14	12	10
50 – 60°N	14	14	14	15	16	17	18	18	18	19	18
40 – 50°N		16	12	19				24	23	21	
30 – 40°N									27	24	
20 – 30°N									29		
Summer											
80 – 90°N		17	19							20	21
70 – 80°N			24	22	21	20				25	
60 – 70°N	24	25	24	24	23	23	26	27	25	27	25
50 – 60°N	28	26	28	28	30	26	27	28	31	31	32
40 – 50°N		27	30	33				31	33	33	
30 – 40°N									24	30	
20 – 30°N									25		
Autumn											
80 – 90°N		23	23							24	24
70 – 80°N			26	25	28	27				24	
60 – 70°N	26	27	29	27	28	23	17	18	21	24	26
50 – 60°N	28	29	29	25	26	20	18	21	23	25	26
40 – 50°N		32	30	23				24	24	24	
30 – 40°N									35	29	
20 – 30°N									34		

Notes: the maximum in each season is shown with a yellow highlight.

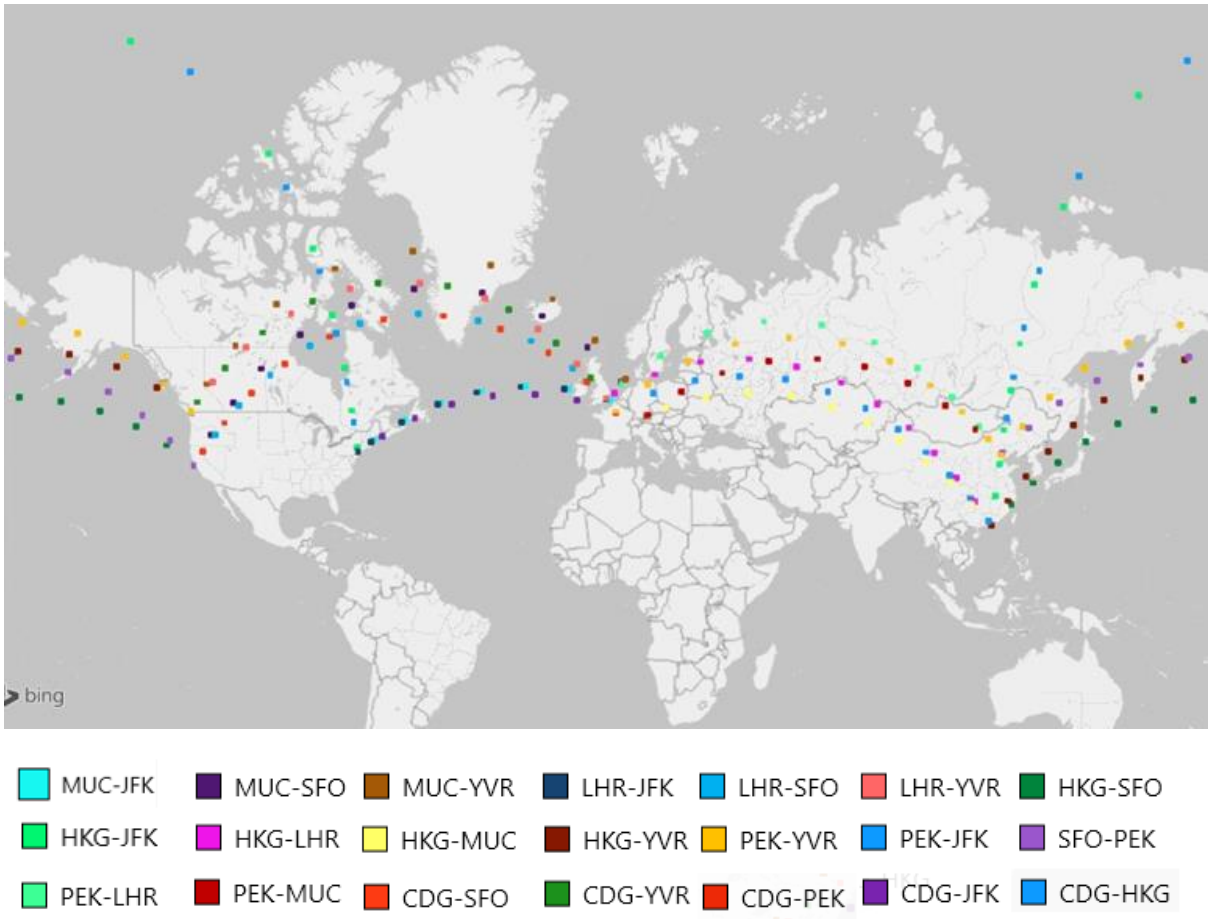

Figure 1. Locations of the hourly points on 21 intercontinental flight paths in which 11 left Europe bound for North America and Asia and 10 left Asia bound for Europe and North America. Details of the three-letter airport codes are given in Table 1.

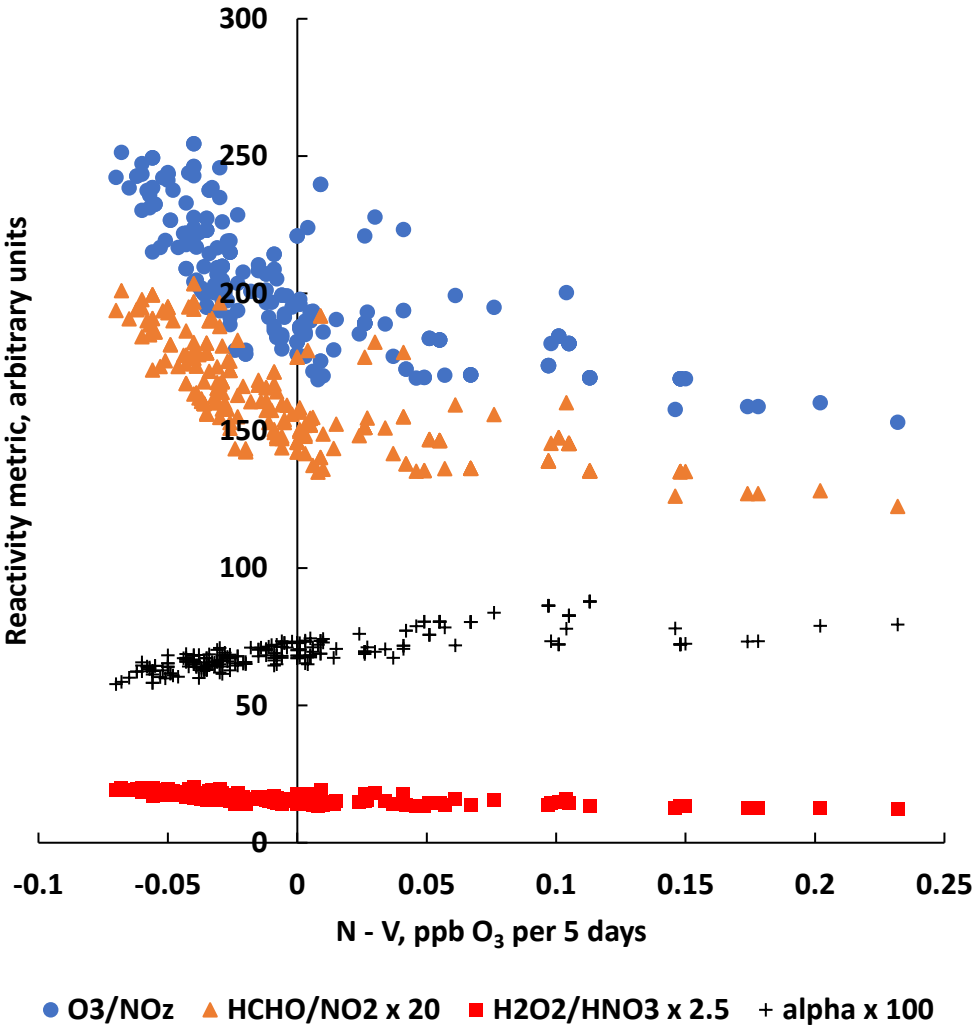

Figure 2. Scatter plot of N – V versus four independent indicator species and their ratios for the 235 flight path locations, showing the reactivity metric O_3/NO_z (filled circles), $HCHO/NO_2$ (scaled by a factor of 25, filled triangles), H_2O_2/HNO_3 (scaled by a factor of 25, filled squares) and α^{CH3O2} (scaled by a factor of 100, plus signs).

a. January

b. April

c. July

d). October

Figure 3a-d. NO_x – O_3 impact metric $\partial O_3/\partial NO_x$ in ppb ppb^{-1} per 5days for each hourly flight path location during each season in the intercontinental air traffic corridors.

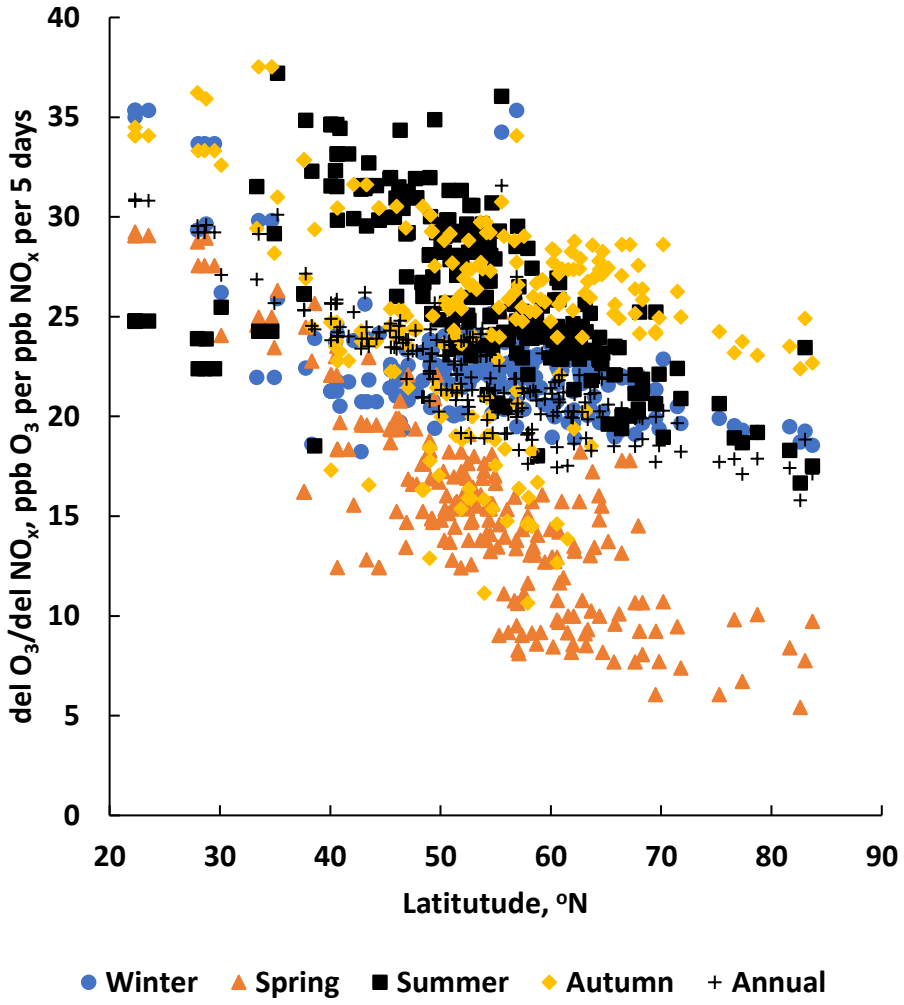

Figure 4. A scatter plot of the impact metric $\partial O_3/\partial NO_x$ in ppb O_3 per ppb NO_x per 5 days versus latitude in ºNorth, showing winter points (filled circles), spring (filled triangles), summer (filled squares), autumn (filled lozenges) and annual points (plus signs).

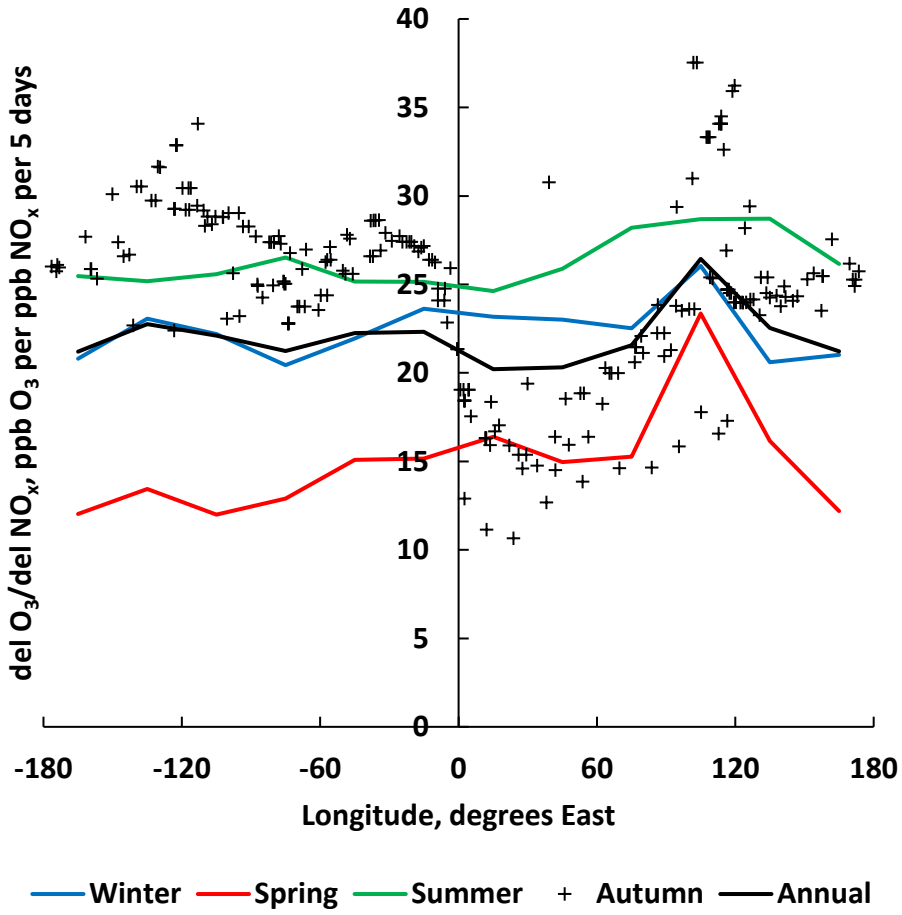

Figure 5. Scatter plot of $\partial O_3/\partial NO_x$ versus longitude (plus signs) for autumn overplotted with the corresponding winter, spring, summer and annual data versus averaged longitude in 30° degree bins (coloured lines).

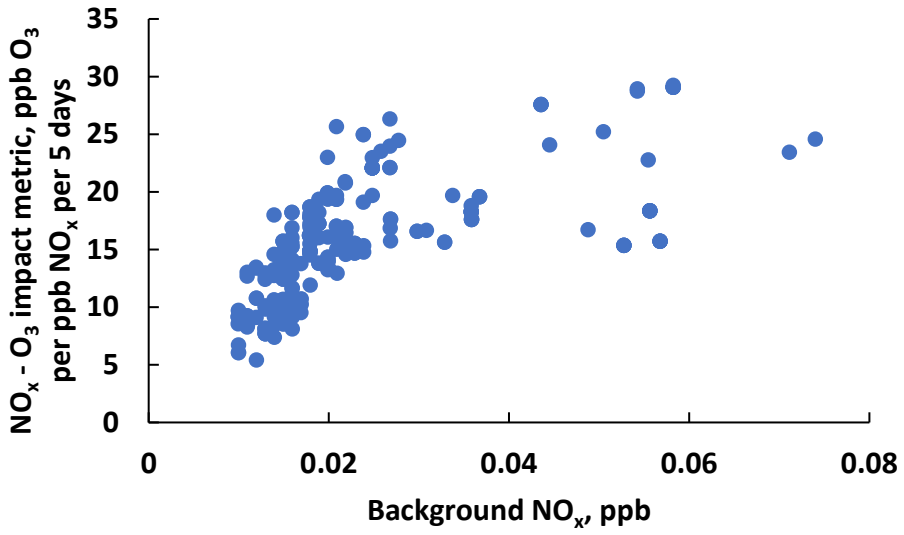

Figure 6. Scatter plot of the NO_x – O_3 impact metric versus background NO_x for spring conditions for the 235 flight path locations.